




Parallel-plate compression test for soft materials: confocal microscopy-assisted ferrule-top nanoindentation

DEXTER MANALILI,^{1,2,*}  MASSIMILIANO BERARDI,¹ HILDE AARDEMA,³ KONSTANTINA ASIMAKI,³ RAYMUND SARMIENTO,⁴ AND B. IMRAN AKCA¹

¹*LaserLab, Vrije Universiteit Amsterdam, De Boelelaan, Amsterdam 1081 HV, The Netherlands*

²*Physics Department, University of San Carlos, Talamban, Cebu City 6000, Philippines*

³*Department of Farm Animal Health, Faculty of Veterinary Medicine, Utrecht University, Yalelaan 7, 3584 CL Utrecht, The Netherlands*

⁴*Department of Biology and Environmental Science, University of the Philippines Cebu, Cebu City 6000, Philippines*

*dexter.manalili@gmail.com

Abstract: The parallel-plate compression test is one of the simplest ways to measure the mechanical properties of a material. In this test, the Young's modulus (E) and the Poisson's ratio (ν) of the material are determined directly without applying any additional modelling and parameter fitting in the post-processing. This is, however, limited when dealing soft biological materials due to their inherent properties such as being inhomogeneous, microscopic, and overly compliant. By combining an interferometry-assisted parallel-plate compression system and a confocal microscope, we were able to overcome these limitations and measure the E (315 ± 52 Pa) and ν (0.210 ± 0.043) of fixated and permeabilized bovine oocytes.

© 2022 Optica Publishing Group under the terms of the [Optica Open Access Publishing Agreement](#)

1. Introduction

Cell mechanobiology has captured increasing interest from different fields for investigating and understanding cell physiology and pathology [1–3]. It connects cellular processes and the mechanics of the cell including elasticity, stiffness, viscoelasticity, and adhesion. Several measurement techniques have been developed to measure cellular mechanics [4–9]; however, most of them are complicated techniques that can provide the actual mechanical properties of the sample only by applying the correct mechanical model. The compression test, on the other hand, is a simple technique which was originally developed for examining the mechanical properties of macroscopically homogeneous engineering materials. This test reveals key properties of the sample by following a straightforward procedure without using additional modelling or parameter fitting.

However, in dealing with soft materials like soft biological tissues and cells, compression tests encounter significant limitations due to the inherent physical properties of these samples. Biological material testing is usually done on the tissue level or down to the cellular scale, which requires more precise dimensional measurements that render mechanical devices less applicable. Additionally, these samples easily comply with minute forces and tend to bend from their own weight, giving them irregular shapes while being unable to supply enough response. The conventional parallel plates with elastic moduli of MPa-GPa would crush these soft materials (0.1-100 kPa [10]) with little to no sensing of mechanical response at all. Lastly, biological materials are far from being homogeneous with each part having local mechanical properties that could be different from the global values requiring multiscale and correlative methods to be modelled properly. In order to break these limitations, we introduce a new compression test by

combining the sensitivity and precision of a ferrule-top nanoindentation system with the optical sectioning capability of a confocal microscope.

We used bovine oocytes as the sample. There is a growing interest towards developing quantitative techniques to measure the mechanical properties of oocytes and embryos both in humans and animals. Previous work showed that there is a strong correlation between oocyte/embryo mechanical properties and their competency in in vitro fertilization treatment (IVF) [11–13]. Our method can provide this quantitative information.

2. Theory of parallel-plate compression test

In this test, the sample is sandwiched in between two rigid plates and then slowly compressed. Simultaneously, the load and the displacement are continuously recorded and then plotted onto a graph. The slope gives the stiffness value of the sample. Dividing the load by the area of contact region and changing the displacement into strain, the Young's modulus (E) is calculated as

$$E = \frac{\sigma}{\varepsilon_z} = \frac{F/A}{(z - z_i)/z_i} = \frac{F/A}{\Delta z/z_i} \quad (1)$$

where σ is the engineering stress in Pa, ε_z is the axial strain (along the axis of the force exerted), F is load in μN , A is the contact area between the plate and the sample in μm^2 , z_i is the initial sample height in μm , and z is the compressed height in μm [14–16]. The Poisson's ratio ν , which is another important material property, can also be directly determined by using the formula

$$\nu = -\frac{\varepsilon_w}{\varepsilon_z} = -\frac{\Delta w/w_i}{\Delta z/z_i} \quad (2)$$

where ε_w is the lateral deformation, Δw is the change in the width when compressed, and w_i is the initial sample width. Equation (2), however, is only applicable when the deformations are infinitesimal ($\sim 1\%$) [17,18]. Since this study involves compression of the sample by up to $\sim 20\%$, it is more accurate to present the calculations of ν using the true strain ϵ instead of the engineering strain ε in Eq. (2). The ϵ is defined as [19]

$$\epsilon_z = \int_{z_i}^z \frac{dz}{z} = \ln\left(\frac{z}{z_i}\right) = \ln(1 + \varepsilon_z) = \ln(\lambda) \quad (3)$$

where λ is the extension ratio. ν can then be calculated as [20,21]

$$\nu = -\frac{\epsilon_w}{\epsilon_z} = -\frac{\ln(1 + \varepsilon_w)}{\ln(1 + \varepsilon_z)} = -\frac{\ln(\lambda_w)}{\ln(\lambda_z)}. \quad (4)$$

The E and ν values, along with the moduli that can be derived from them, are enough to characterize the mechanical behavior of linear homogeneous isotropic material [22].

3. Method

3.1. Measurement setup

The compression setup used in this experiment is illustrated in Fig. 1. The two major parts are the ferrule-top nanoindentation system and the confocal microscope. The monolithic indentation system is based on the previous work of Prof. Iannuzzi's group [23–26]. The all-optomechanical characteristics of this system make it ideal for examining samples that are permanently immersed in liquid. The indentation system consists of four components: the xyz-axes micromanipulator (PatchStar, Scientifica) for coarse position control of the indenter, the piezoelectric manipulator (P-602.5SL, Physike Instrumente GmbH) for fine positioning of the indenter in the z-axis, the interferometer with a tunable laser source centered at $\lambda=1550$ nm (OP1550, Optics11) to monitor

the bending of the cantilever and the ferrule-top indenter to probe the sample. A single-mode optical fiber attached to the side of the ferrule continuously measures the bending of the cantilever $d_{cantilever}$ by sending the Fabry-Pérot (fiber-water to water-cantilever cavity) signal back to the interferometer. This operation, along with the positioning of the piezo d_{piezo} enables the system to constantly measure the level of indentation or compression $d(t)$ at any time by following

$$d(t) = d_{piezo}(t) - d_{cantilever}(t) \quad (5)$$

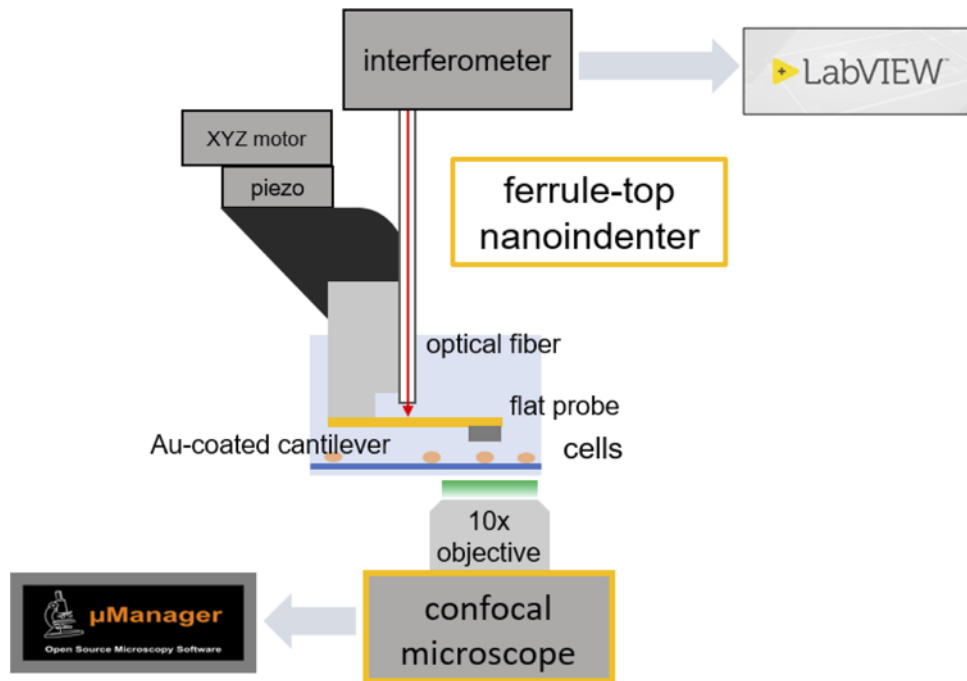


Fig. 1. Schematic of the confocal microscope assisted ferrule-top nanoindentation system. The ferrule-top indenter is used to compress cells from the top and the confocal imaging system takes three dimensional scans from the bottom. The two components operate independently from each other and are controlled by separate programs: indenter by LabVIEW and confocal imaging by μ Manager. The flat probe and the glass bottom of the confocal dish form a parallel-plate compression test setup for the cells. The cantilever deflection is monitored by a single-mode optical fiber that is connected to an interferometer.

The operating functions of the indentation system components are all integrated in a LabVIEW program. This means that a feedback loop that reads the cantilever bending and controls the piezo can be used to keep the compression level constant. The program also records and saves the loads and positions of the piezo and the cantilever bending into a single file for data analysis.

The central element of the imaging system is the re-scanning confocal microscope (RCM, Confocal.nl). The RCM offers an improvement of $\sqrt{2}$ in the lateral resolution over the conventional one and fully integrates the CMOS camera (ORCA-Flash 4.0 V3, Hamamatsu), the tunable laser source (iChrome MLE, Toptica Photonics), the microscope (Diaphot-TMD, Nikon) and the computer altogether into a single μ Manager interface. The laser source can be tuned to lines 405 nm, 488 nm, and 640 nm depending on the excitation wavelength of the dye used with the sample. In addition, the CMOS camera active frame can be set to smaller sizes, which consequently increases the scanning rates up to 4 fps. A 10x objective lens (Plan Fluorite 0.5 NA, Nikon)

is equipped onto the microscope to cover the entire volume of the bovine oocytes (diameter 130-180) μm in a single field of view.

The indenter and the imaging system operate independently from each other; therefore, the setup can be easily transformed with a different mechanical technique or with a different 3D-imaging technology. This modular characteristic makes this technique flexible for a wide range of applications.

3.2. Experimental procedure

3.2.1. Oocyte preparation

The technique presented in this study is tested on fixed bovine oocytes. Cumulus-oocyte-complexes were collected from bovine slaughterhouse ovaries (rest material) and were matured for 23 hours according to the previously described method in [27]. After maturation, the cumulus cells that surround the oocyte were removed and the oocytes were fixed with 4% paraformaldehyde (PFA) diluted in Dulbecco's phosphate-buffered saline (DPBS). After an incubation period of 30 minutes in 4% PFA, the samples were washed 3 times with DPBS. A permeabilization (0.1% Triton X-100) solution was added to the DPBS medium, followed by an incubation of 15 minutes. After removing the permeabilization solution and washing with DPBS 3 times, the cells were then stained with 2 $\mu\text{g}/\text{mL}$ HCS CellMask Green (Invitrogen) stain solution. The final stage of preparation was washing the oocytes with DPBS 3 times after an incubation period of 40 minutes. More DPBS is then added to fill up the petri dish because the following steps are done while the sample and the indenter are fully immersed in liquid. The cells are then allowed to attach to the glass bottom for around 20 hours. The oocytes are examined on the same day of their preparation.

3.2.2. Cell compression

The flat glass probe that was used for cell compression was obtained by cutting a microscope glass slide into pieces and gluing one of the opposing smooth sides to the cantilever. This flat probe forms a parallel-plate compressor with the glass bottom of a confocal dish (TC-treated, VWR). These glass plates have significantly higher elastic moduli (61-72 GPa [28]) compared to soft biological materials (0.1-100 kPa) and can thus be considered rigid in these experiments. In this case, only the sample deforms during compression and the bending of the cantilever should not be significant enough to cause a non-uniform load distribution. The recorded loads can also be then directly attributed to the deformation of the sample.

The cell compression is done by moving the flat probe downwards following the sample profile shown in Fig. 2. The cell is compressed by 1 μm first and is kept at that level for 30 seconds but no images are taken. The cell is again compressed by another 1 μm and after 30 seconds, its volume is scanned by the confocal microscope for about 4-5 minutes. The 30 seconds is used as a stabilization time. It is a time given to the cantilever and the piezo to stabilize their positions and keep the compression level constant using Eq. (5). The load and position of the piezo and the bending of the cantilever are continuously recorded by the LabVIEW program. Based on preliminary experiments, the stabilization time is dependent on the size and shape of the probe. For the flat probe in use, the stabilization time of 30 seconds was found to be optimal even at higher compression levels. This procedure repeats at different compression levels up to 36 μm but the imaging is not done on every one of them. It is worth noting that the non-imaging compression levels increases with depth and the reason for that is it takes longer for the system to stabilize as the cell gets more compressed and these intermediate levels provide "resting" periods.

3.2.3. Imaging

The cell stain is excited by tuning the laser source to a wavelength of 488 nm. The laser is set to 1% of its total power to prevent electronic saturation of the camera and to minimize fluorophore depletion. The axial distortion due to refractive index mismatch between the immersion medium

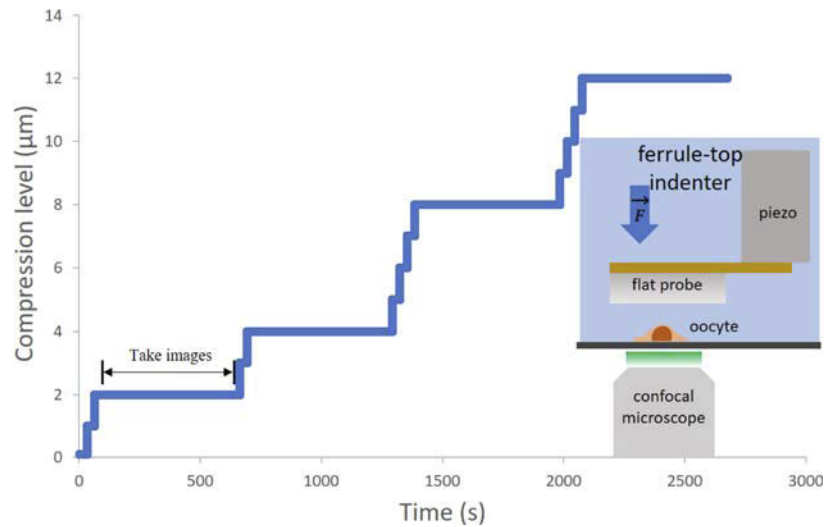


Fig. 2. Sample compression profile. The piezo is dictated by the LabVIEW program to move downwards at an interval of $1 \mu\text{m}$ and speed of $20 \mu\text{m/s}$. Upon reaching user-defined levels, the system keeps the depth constant by continuously balancing the position of the piezo and the bending of the cantilever. This gives time for the confocal microscope to scan the entire volume of the sample.

and the objective lens immersion (air) is not emphasized in this study for two reasons: 1) low NA (0.5) aberrations have less effect on confocal images [29] and, more importantly, 2) calculations involving axial measurements, such as the axial deformation and the Poisson's ratio, are normalized with respect to the initial axial dimension (which is also distorted by the same factor) thereby cancelling any effect in the resulting value. The images are $512 \text{ pixels} \times 512 \text{ pixels}$ with pixel size of $0.65 \mu\text{m} \times 0.65 \mu\text{m}$ and an axial separation of $1 \mu\text{m}$, recorded at 1.1 frames per second.

3.3. Data analysis

The confocal images are saved in stacks, one for each imaging compression level. Each of the stacks is analyzed using standard Fiji/ImageJ functions with the procedure adopted from [30]. The images are first processed with a 2-dimensional median filter to help define the edges. Next, background subtraction is applied using a rolling ball method to correct the uneven background illumination. The images are then smoothed using a 2-D Gaussian filter. Finally, the pixel values are thresholded automatically using the default algorithm for a more robust and consistent process.

As shown in Fig. 3, the fluorescent signal from the Zona Pellucida (ZP) is indistinguishable from the background. One way to include the ZP is to lower the intensity threshold value during the final step. The result is shown in red in Fig. 4. In doing so, some of the background noise gets included and it makes measurements more complicated and less precise. To simplify things, only the cytoplasm (yellow) is considered further in this work. This means that the experiments are carried out on whole oocytes but only the dimensions and properties of the cytoplasm are measured. In a way, the technique in this study exploits the optical sectioning capability of the confocal microscope by being able to examine a region within a sample without physically isolating it from the whole. This technique could be handy in investigating different parts simultaneously within a sample, provided that these parts are stained properly and have well-defined boundaries. Potentially, this means that its applications can be extended to

investigating cell physiology. In the case where the nucleus and the cytoplasm are stained with different dyes that are excited at different wavelengths, it should be possible to examine both of them simultaneously through proper image processing procedures.

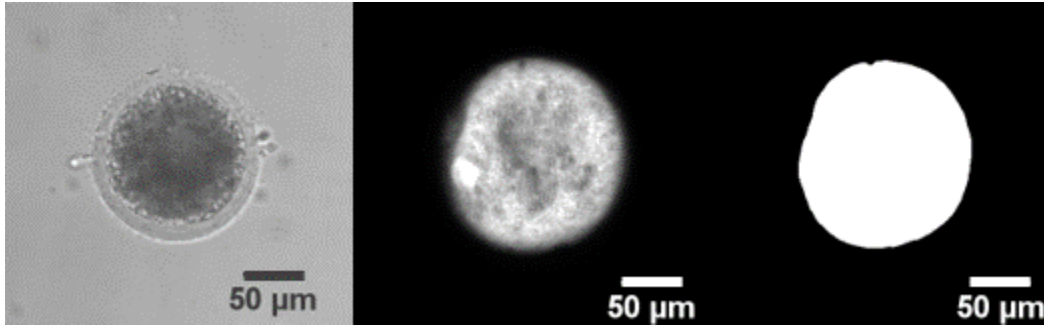


Fig. 3. Images of fixed bovine oocyte stained with HCS CellMask Green under an optical microscope (left), confocal microscope with 488 nm as excitation wavelength (center), and (right) after image processing. The raw confocal image (center) suggests that the dye was not effective in staining the ZP, about 100x less fluorescent than the cytoplasm. Note that the oocyte on the left is different from the one in the center and right panels.

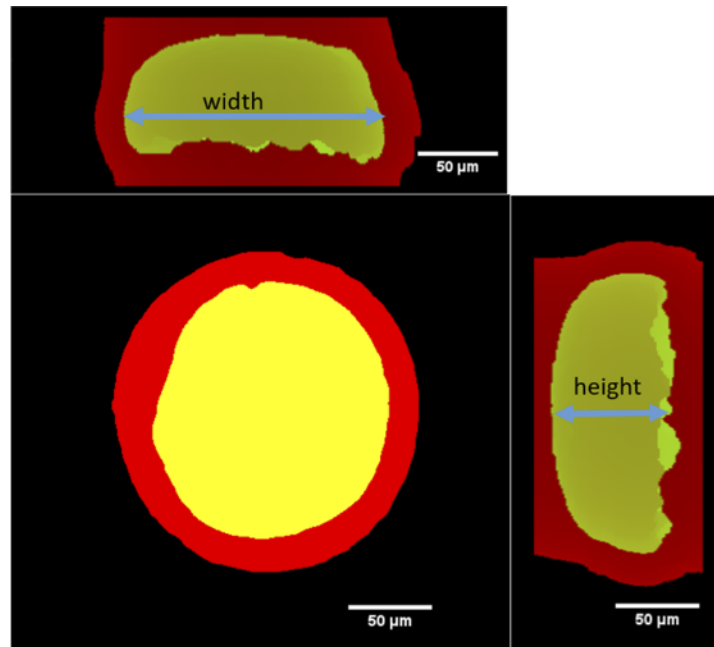


Fig. 4. Oocyte 3D reconstruction from the confocal images. Yellow is the resulting image after the standardized image processing; red is an attempt to reconstruct the entire oocyte by lowering the threshold intensity value to include the zona pellucida (ZP). With the red image being clipped and unable to distinguish the zona pellucida from the background, only the cytoplasm (yellow) is considered in further measurements. The dome shape of the of the cytoplasm is due to the fact the it was allowed to attach to the glass bottom of the petri dish for around 20 hours. It is also worth noting that the oocytes in this experiment are fixated and permeabilized and may therefore have shapes different from the live ones.

As explicitly shown in Eqs. (1)–(4), three parameters are needed to determine the E and ν values: height, width, and contact area. Deformations in the height and width will be used to calculate the ν while the contact area is divided from the piezo load to determine the stress value or the E calculations. Note that the contact area in these experiments is measured at every level and not assumed to be equal to the initial contact area, unlike in the compression tests for regular materials. Instead of engineering stress, therefore, this study measures and uses the true stress, which is more useful in measuring the fundamental properties of the material [31,32].

The dimensions of the sample are measured after the image processing had been implemented. After processing the images, the frames are stacked and interpolated along the z -axis to form a 3D reconstruction of the sample. Dimensions are measured in pixels and then converted to metric units. The height and width are measured by projecting the 3D-reconstructed image in the x -axis and z -axis, respectively. Both of these projections are analyzed through the use of a plot profile, as shown in Fig. 5. The dimensions are determined by measuring the width of their profiles as shown in Fig. 5(B) and 5(D). The conversion factor from pixel to μm is the camera pixel size divided by the magnification of the objective lens. The height is measured only in one orientation while the width is measured at 5 different lateral orientations: at angles 20 degrees away from one another about the z -axis. This is especially important for experiments that aim to investigate the anisotropy of the sample. Mechanical anisotropy of cells has already been shown in [33,34].

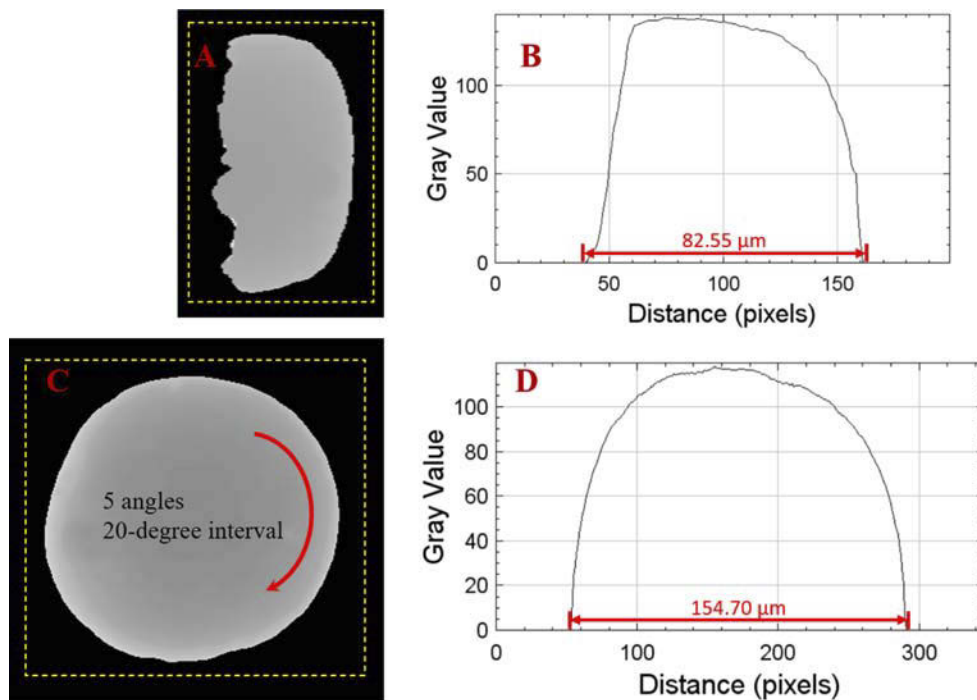


Fig. 5. Measuring the height and width of the oocyte from the y - z (A) and x - y (C) projections, respectively. The dimensions are measured by marking the boundaries of the intensity plot profile. The difference between these markers, which is in unit pixels, is then converted to microns. The profile width in (B) gives the height while in (D), it gives the width/diameter of the sample. The projection in (C) is then rotated by 20 degrees 4 times to measure the widths in different orientations.

To investigate this, ν shall be determined at every lateral orientation n and takes the form

$$\nu_{zn} = \frac{\epsilon_n}{\epsilon_z} \quad (6)$$

where ν_{zn} and ϵ_n are the Poisson's ratio and the true strain for different n , respectively [35,36]. Instead of a line, a box is used to span both the height and the widths in Fig. 5(A) and 5(C). In this way, the gray values in the vertical axis are averaged and selecting a specific line is no longer needed. This is a convenient way to measure the width because there is no need to specify a geometrical center. Since the images are already binary after the image processing, it is easy to identify the boundaries.

A simpler approach is used to measure the area. Instead of relying on the 3D-reconstructed image, this procedure relies on pixel counting. Each of the frames in the stack are scanned and the number of pixels are counted and converted to square microns using the Fiji plugin *Voxel Counter*, which was originally made to measure volumes [37]. The plugin tabulates the areas of the frames within the stack. The widest area in the list is chosen for calculating for the Young's modulus because that is where the deformation is largest. The location of this area has been observed to go downwards as the oocyte got more compressed.

4. Results

Shown in Fig. 6(A) are projections of an oocyte cytoplasm at different levels of compression. From panel (i) to panel (ii), the transformation due to compression can already be observed but it is only panel (iii) where the flattening is starting to become more apparent. It is no coincidence that the bottom part of the cytoplasm gets flatter as it gets more compressed since it is already in contact and attached to the glass bottom of the petri dish.

The measured pre-compression dimensions; width, height and widest area, of the bovine oocytes (mean \pm SD) were $76.3 \pm 2.9 \mu\text{m}$, $156.7 \pm 1.6 \mu\text{m}$ and $43552 \pm 1319 \mu\text{m}^2$, respectively. The width values are taken from 15 measurements (3 oocytes \times 5 orientations). Due to instability of the indenter at larger axial strains during practice experiments, only the data up to 20% axial strain are considered and used for calculations of the E and ν values. The width and the widest area are constantly increasing as the cell got more compressed, which suggests that the ν is positive. Pairing the big size of the oocytes with the piezo's high axial resolution of 3 nm effectively increases the range at which linear deformation can be done.

From the engineering and true stress-strain curves in Fig. 6(C), the Young's moduli are $315 \pm 52 \text{ Pa}$ and $249 \pm 44 \text{ Pa}$, respectively. The Poisson's ratios from the engineering strain in Eq. (2) and true strain in Eq. (4) are 0.210 ± 0.043 and 0.182 ± 0.039 , respectively. The mean values are averaged from the 3 oocytes, each with 5 measurements. The errors presented are calculated via error propagation. Although the anisotropy of the oocytes is considered in the analysis, it is hard to pinpoint the reason behind such behavior because the oocytes are all fairly circular and the images in this study are limited in terms of internal structural information; unlike in [32] where the cells are elliptical and the anisotropy can be attributed to the orientation of the actin stress fibers. The standard deviation of the measured deformations along different orientations is less than the width of 1 pixel ($0.65 \mu\text{m}$) which means that there is no significant display of anisotropy. This also implies that the other isotropic material properties of the oocytes, such as the shear modulus and bulk modulus, can be calculated from the determined Young's modulus and Poisson's ratio.

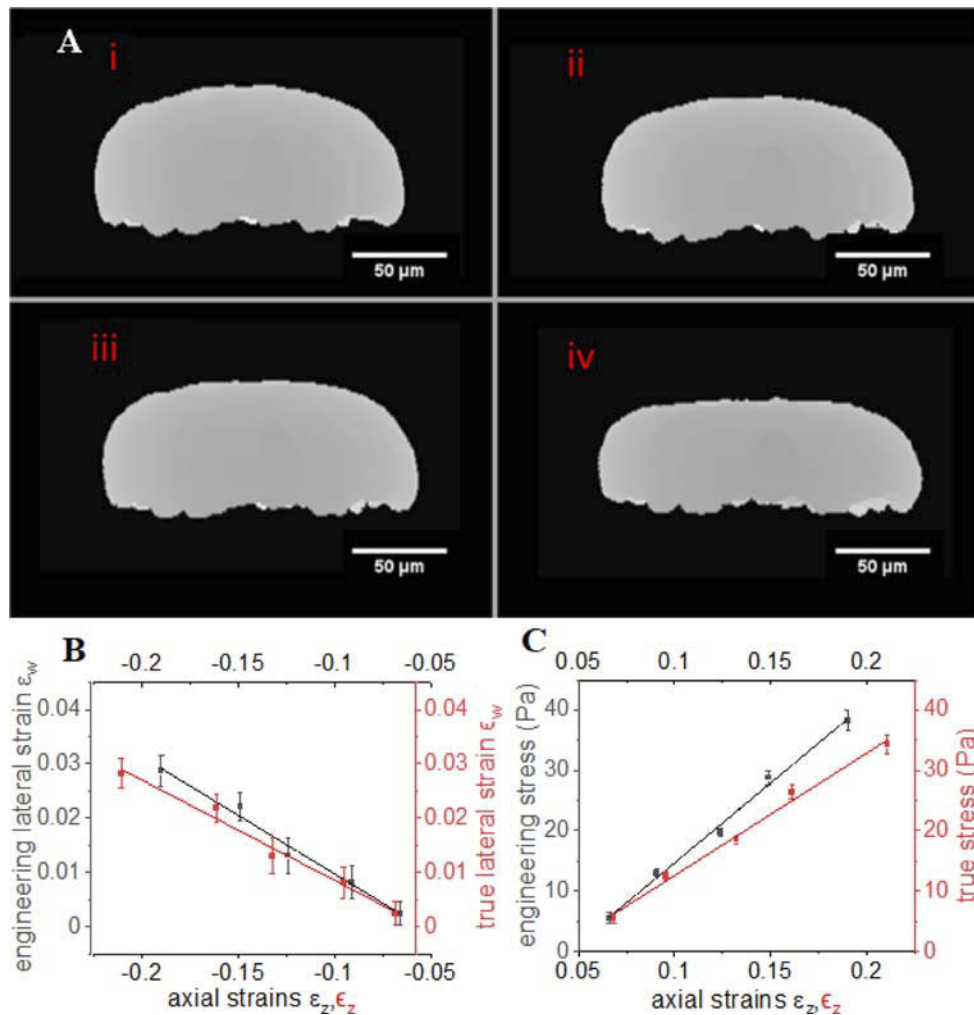


Fig. 6. (A) Projections of the cytoplasm as the cell is compressed by (i) 0 μm , (ii) 4 μm , (iii) 12 μm , and (iv) 30 μm . The widening of the sample is apparent as it gets more compressed. The flattening of the bottom part in panels (iii) and (iv) is expected, given that the cell is pressed against the glass bottom of the petri dish. (B) Lateral strains as functions of the respective axial strains for both infinitesimal (black) and finite (red) deformation considerations (mean \pm SD, $N = 5$). The slopes of the linear fits are the negative values of the respective Poisson's ratios. (C) Engineering and true stress-strain curves from a cell compression test (mean \pm SD, $N = 5$). Absolute values are used in the x-axis. The slopes of the linear fits are the respective Young's modulus. The data can be found at [Dataset 1](#) [45].

5. Discussion

This study has similarities with the technique presented in [34]. Both present methods of investigating how cells behave under compression and both are combinations of an indenter and a confocal microscope. However, there are key differences that set these experiments apart from each other. First, the indenters used in these studies work differently. Whereas the indenter in the mentioned literature is like a miniaturized version of the compression setup for regular materials, the indenter in this study is aided by interferometry that enables it to actually detect when the probe of the indenter makes contact with the sample. This event is denoted by a "spike" in the

signal coming from the interferometer. Even if the glass probe reflects some of the light, it is easy to distinguish the top of the cytoplasm from it since they are separated by the relatively low fluorescent ZP which is approximately $20\ \mu\text{m}$ thick. Another difference is how the axial deformations are being measured, which is a consequence of the first one. The axial strain in this study is determined purely from the confocal images unlike in the literature where it is dependent on the position of the piezo. An important advantage of the indenter used in this study is the ability to control the compression level while the confocal microscope scans the entire volume of the sample. This is especially important when dealing with soft biological materials that could relax after the load has been applied. Keeping the compression level ensures that the height of the sample is kept constant while it is being scanned by the confocal microscope. The measurement of the axial deformation is essential in the precise calculations of both the Young's modulus E and the Poisson's ratio ν . In both of these studies, the use of confocal imaging makes the need for assumptions of the cell's geometry unnecessary. Another point that separates this study from the current literature is that the values of ν here are measured and not assumed to be 0.5. Note that $\nu = 0.5$ implies incompressibility of the sample, which is not the case in this experiment. All three cells decreased in volume due to compression up to a certain level. The highest volume reduction recorded in this study is 5.1%, caused by a 19.0% axial strain. The volume is measured via the Fiji plugin Voxel Counter which sums up all the volumetric pixels (voxels) found in a confocal scan.

In order to characterize the mechanical behavior of a sample under compression, at least two properties need to be determined [38]. In this study, the E and ν values are determined by measuring the deformations in the width, height, and area. These dimensions are all purely measured from the 3D-reconstructed image of the sample via confocal imaging. Only the force to calculate the E was measured mechanically. The downside of relying fully on imaging in measuring dimensions is that it is limited by the resolution of the imaging technique. For 3D imaging, especially, there is an additional problem of distortion along the optical axis [29,39]. However, it can be fairly assumed that this distortion is uniform all throughout the sample, regardless of depth. This means that as long as this premise stands, measuring the right dimensions along the optical axis is just a matter of finding the linear z-factor to correct the distortion. Thankfully, this problem is not an issue when measuring normalized parameters such as strains. The distortion factor vanishes as the change in dimension is divided by the initial value since both of them are distorted by the same factor. In this study, the distortion factor is not necessary to measure the axial strain. It is important to note, however, that any (0,0) data point involving the axial strain should be excluded from the analysis. All the other data points in the set scales with the distortion factor, except the (0,0). Depending on the scaling factor, any curve with the axial strain as the x-axis will either move to the left or to the right. In any of these cases, the (0,0) remains bounded at the origin. Excluding the (0,0) ensures that the slope of the dataset does not change with the distortion factor. This is an essential part in the data analysis since the E and ν are the slopes of the stress-strain and the lateral strain-axial strain curves, respectively.

As shown in Fig. 6(A), the oocyte is visibly flattened and widened as it gets more compressed. Qualitatively, this already means that ν is a positive value. To quantify this, the changes in the height (axial) and width (lateral) are measured at every compression level. Shown in Fig. 6(B) are the lateral strain-axial strain curves for both infinitesimal (black) and finite (red) strain values used in Eqs. (2) and (4), respectively. The infinitesimal ν is calculated to be 0.210 ± 0.043 while its finite counterpart is 0.182 ± 0.039 . The values presented have not been compared to other results due to scarcity of available literature, most assign the value to be 0.5 for simplicity of calculations and for the fact that cells are around 70% water.

Modelling the cells as compound structures made of water and solid components, the effective ν can then be approximated as

$$\nu = c_w \nu_w + (1 - c_w) \nu_s \quad (7)$$

where c_w is the percent water content, ν_w and ν_s are the Poisson's ratios of water and the solid component, respectively ($\nu_w = 0.5$). For cells with 70% water, $\nu = 0.5$ if and only if the solid part is also incompressible but is rarely the case. Solids can also have negative values of ν (auxetics) [40]. The resulting values for ν in this experiment imply a few possibilities: (a) the water remains inside the oocytes and the solid component is highly auxetic, (b) a huge amount of water leaks out of the cell and the solid component has $\nu \geq 0$, and (c) a small amount of water leaks out and the solid component is mildly auxetic. Considering the harsh processes involved in preparing the oocytes for the experiments, either (b) or (c) is more probable to be the case due to the exodus of water through the holes in the cell membrane left by the fixation and permeabilization processes [41]. As the cells get more compressed, the more water is excreted. This can be checked with an experiment on live oocytes which are too delicate for the current setup.

The E values, slopes of the linear fits in Fig. 6(C), from the engineering stress-strain and true stress-strain curves are 315 ± 52 Pa and 249 ± 44 Pa, respectively. Reported values from previous studies are in the order of 1-100 kPa, depending on the maturity stage oocyte [42] and the type of test used (AFM [43,44] or micropipette aspiration [27]). It is important to note, however, that these experiments: 1) only focused on measuring the localized mechanical properties of the ZP while this experiment measures the cytoplasm, and 2) assigned a value for the ν to either 0.5 (incompressible) or 0.3. By assigning $\nu = 0.5$, the deformations are automatically assumed to be infinitesimal and the volume invariant, which are not the case in this study. Shown in Fig. 7 is the comparison of the actual change in volume of an oocyte to geometrical approximations. This graph highlights the importance of direct measurements. This also shows that, while logical, geometrical approximations do not always result to a precise representation of the actual transformation.

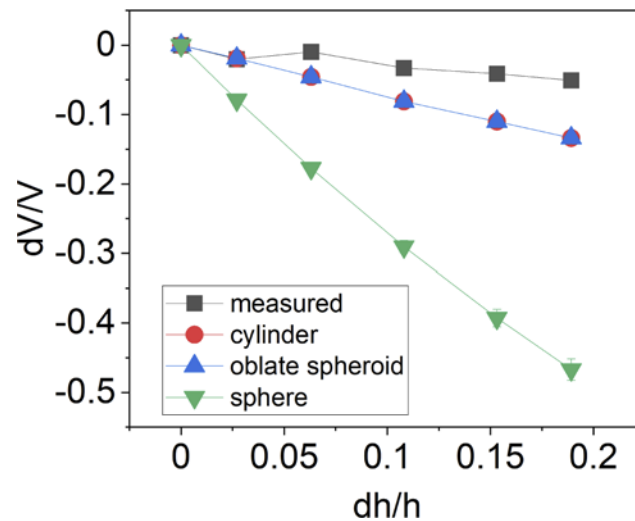


Fig. 7. The measured fractional change in volume compared to oblate spheroid, cylindrical, and spherical approximations given the changes in the height of an oocyte due to compression. A $\sim 19\%$ compression only corresponds to a measured 5% change in volume while it is more than doubled in both geometrical calculations.

As with any other method, this technique comes with disadvantages. Mainly, the dimensional measurements in this paper rely heavily on the resolving power of the confocal microscope and the shorter the excitation wavelength, the better the resolution. A shorter wavelength, however, corresponds to a shallower penetration depth. Even for longer wavelengths, it is still important to note how much light is absorbed and scattered due to the optical properties of the sample.

The next challenge is to find the right dyes for the samples and for specific applications. The penetrability of the staining solution matters a lot. The dye used in this experiment is membrane impermeant thereby requiring the oocytes to be fixated and permeabilized for it to be effective. Using proper staining solutions will make it possible to measure live samples. Multiple dyes can also be used to simultaneously examine multiple regions within a sample, given that the dimensions are within the resolution of the microscope and the excitation wavelengths of the dyes are available in the setup. It is worth noting that the results for the E and ν are from the measurements on fixated and permeabilized oocytes. This means the structural integrity of the cell is compromised and the measured mechanical properties should not be used to represent live oocytes. An experiment on live samples with proper membrane permeant dyes should be carried out to obtain results relevant to actual biological applications such as in vitro fertilization (IVF) and bioengineering. This research is done almost purely to demonstrate the technique presented. Experiments on phantoms would have been a solid addition to the data presented in this paper. There were several attempts to make 3D printed polymer samples that are suitable for our setup in terms of stiffness and compatibility with staining but the least stiff structure that was synthesized was still too stiff for the existing setup. Unfortunately, we could not acquire any data using these phantoms.

6. Conclusion

To summarize, this study introduces a new method of measuring mechanical properties of soft biological materials under compression. The technique can be viewed as a miniaturized engineering compression test that is developed for soft materials. The sensitivity of the interferometry-aided indentation system and its capability to control the compression level play a fundamental role in making this technique work. The optical sectioning feature of the confocal microscope is the key to measuring the deformations and the localized mechanical properties of a sample that is within a bigger sample, such as the cytoplasm or ZP. As already mentioned, it could be possible to measure more parts simultaneously as long as these parts are stained properly and have well-defined boundaries. The values of E and ν were measured from fixated and permeabilized oocytes and cannot be translated to the corresponding values for the live ones. Lastly, it is very important to note that the mechanical properties presented in this study are all taken from measured quantities and no additional modelling and parameter fitting were needed to determine their values.

Funding. Science Education Institute, Department of Science and Technology, Republic of the Philippines.

Acknowledgments. The authors gratefully acknowledge the contributions of Martin Slaman and Erik Paardekam in the fabrication of the ferrule-top indenter and for technical support, Edcel Salumbides for fruitful discussions, and Prof. Davide Iannuzzi for major support since the conceptualization of this work. This work was partly funded by the Science Education Institute, Department of Science and Technology, Republic of the Philippines under the Accelerated Science and Technology Human Resource Development Program's "Sandwich Program Grant".

Disclosures. The authors declare no conflicts of interest.

Data availability. Data underlying the results presented in this paper are available in [Dataset 1](#) [45].

References

1. S. R. Nagel, "Experimental soft-matter science," *Rev. Mod. Phys.* **89**(2), 025002 (2017).
2. Y. L. Wang and D. E. Discher, *Methods in Cell Biology, Volume 83: Cell Mechanics* (Academic Press, 2007), chap. Preface.
3. L. Andolfi, E. Masiero, E. Giolo, M. Martinelli, S. Luppi, S. Dal Zilio, I. Delfino, R. Bortul, M. Zweyer, G. Ricci, and M. Lazzarino, "Investigating the mechanical properties of zona pellucida of whole human oocytes by atomic force spectroscopy," *Integr. Biol.* **8**(8), 886–893 (2016).
4. K. Miller, "Method of testing very soft biological tissues in compression," *J. Biomechanics* **38**(1), 153–158 (2005).
5. Y. R. Zhang, K. J. Xu, Y. L. Bai, L. Q. Tang, Z. Y. Jiang, Y. P. Liu, Z. J. Liu, L. C. Zhou, and X. F. Zhou, "Features of the volume change and a new constitutive equation of hydrogels under uniaxial compression," *J. Mech. Behav. Biomed. Mater.* **85**, 181–187 (2018).

6. D. R. Gossett, H. T. K. Tse, S. A. Lee, Y. Ying, A. G. Lindgren, O. O. Yang, J. Rao, T. Clark, and D. D. Carlo, "Hydrodynamic stretching of single cells for large population mechanical phenotyping," *Proc. Natl. Acad. Sci. U. S. A.* **109**(20), 7630–7635 (2012).
7. J. H. Kang, T. P. Miettinen, L. Chen, S. Olcum, G. Katsikis, P. S. Doyle, and S. R. Manalis, "Noninvasive monitoring of single-cell mechanics by acoustic scattering," *Nat. Methods* **16**(3), 263–269 (2019).
8. L. Guillou, A. Babataheri, P. H. Puech, A. I. Barakat, and J. Husson, "Dynamic monitoring of cell mechanical properties using profile microindentation," *Sci. Rep.* **6**(1), 21529 (2016).
9. D. Hartono, Y. Liu, P. L. Tan, X. Y. S. Then, L. Y. L. Yung, and K. M. Lim, "On-chip measurements of cell compressibility via acoustic radiation," *Lab Chip* **11**(23), 4072–4080 (2011).
10. I. Levental, P. C. Georges, and P. A. Janmey, "Soft biological materials and their impact on cell function," *Soft Matter* **3**(3), 299–306 (2007).
11. Y. Murayama, J. Mizuno, H. Kamakura, Y. Fueta, H. Nakamura, K. Akaishi, K. Anzai, A. Watanabe, H. Inui, and S. Omata, "Mouse zona pellucida dynamically changes its elasticity during oocyte maturation, fertilization and early embryo development," *Human cell* **19**(4), 119–125 (2006).
12. Y. Murayama, M. Yoshida, J. Mizuno, H. Nakamura, S. Inoue, Y. Watanabe, K. Akaishi, H. Inui, C. E. Constantinou, and S. Omata, "Elasticity Measurement of Zona Pellucida Using a Micro Tactile Sensor to Evaluate Embryo Quality," *J. Mammalian Ova Res.* **25**(1), 8–16 (2008).
13. J. Kort and B. Behr, "Biomechanics and developmental potential of oocytes and embryos," *Fertil. Steril.* **108**(5), 738–741 (2017).
14. M. Jerabek, Z. Major, and R. W. Lang, "Uniaxial compression testing of polymeric materials," *Polym. Test.* **29**(3), 302–309 (2010).
15. N. Srivastava, R. R. Kay, and A. J. Kabla, "Method to study cell migration under uniaxial compression," *Mol. Biol. Cell* **28**(6), 809–816 (2017).
16. N. Bui, P. Durand-Smet, and A. Asnacios, "Single-cell mechanics: The parallel plates technique," *Methods Cell Biol.* **125**, 187–209 (2015).
17. Y. Ling, "Uniaxial true stress-strain after necking," *AMP J. Technol.* **5**, 37–48 (2004).
18. A. P. Singulani, "Advanced Methods for Mechanical Analysis and Simulation of Through Silicon Vias," Ph.D. thesis, Technischen Universität Wien (2014).
19. D. W. A. Rees, *Basic Engineering Plasticity: An Introduction with Engineering and Manufacturing Applications* (Elsevier Ltd, Oxford, 2006).
20. I. Scheider, W. Brocks, and A. Cornec, "Procedure for the determination of true stress-strain curves from tensile tests with rectangular cross-section specimens," *J. Eng. Mater. Technol.* **126**(1), 70–76 (2004).
21. C. Vergari, P. Pourcelot, L. Holden, B. Ravary-Plumioën, G. Gerard, P. Laugier, D. Mitton, and N. Crevier-Denoix, "True stress and Poisson's ratio of tendons during loading," *J. Biomechanics* **44**(4), 719–724 (2011).
22. J. M. Tse, G. Cheng, J. A. Tyrrell, S. A. Wilcox-Adelman, Y. Boucher, R. K. Jain, and L. L. Munn, "Mechanical compression drives cancer cells toward invasive phenotype," *Proc. Natl. Acad. Sci. U. S. A.* **109**(3), 911–916 (2012).
23. D. Iannuzzi, S. Deladi, V. J. Gadgil, R. G. Sanders, H. Schreuders, and M. C. Elwenspoek, "Monolithic fiber-top sensor for critical environments and standard applications," *Appl. Phys. Lett.* **88**(5), 053501 (2006).
24. D. Chavan, G. Gruca, S. De Man, M. Slaman, J. H. Rector, K. Heeck, and D. Iannuzzi, "Ferrule-top atomic force microscope," *Rev. Sci. Instrum.* **81**(12), 123702 (2010).
25. D. Chavan, T. C. Van De Watering, G. Gruca, J. H. Rector, K. Heeck, M. Slaman, and D. Iannuzzi, "Ferrule-top nanoindenter: An optomechanical fiber sensor for nanoindentation," *Rev. Sci. Instrum.* **83**(11), 115110 (2012).
26. H. Van Hoorn, N. A. Kurniawan, G. H. Koenderink, and D. Iannuzzi, "Local dynamic mechanical analysis for heterogeneous soft matter using ferrule-top indentation," *Soft Matter* **12**(12), 3066–3073 (2016).
27. M. Berardi, K. Bielawski, N. Rijnveld, G. Gruca, H. Aardema, L. van Tol, G. Wuite, and B. I. Akca, "Optical interferometry based micropipette aspiration provides real-time sub-nanometer spatial resolution," *Commun. Biol.* **4**(1), 610 (2021).
28. Y. An, B. Y. Joo, D.-T. Chung, and S.-Y. Choi, "Finite element simulation of brittle fracture of bulletproof glass system," *J. Mech. Sci. Technol.* **28**(1), 73–80 (2014).
29. S. Hell, G. Reiner, C. Cremer, and E. H. Stelzer, "Aberrations in confocal fluorescence microscopy induced by mismatches in refractive index," *J. Microsc.* **169**(3), 391–405 (1993).
30. N. Condon, "IMB Microscopy," <https://imb.uq.edu.au/microscopy> (2020).
31. Amazon Services LLC Associates Program, "True Stress-Strain vs Engineering Stress-Strain," <https://msestudent.com/true-stress-strain-vs-engineering-stress-strain/> (2021).
32. J. Hiatt, "Stress and Strain," <https://community.sw.siemens.com/s/article/stress-and-strain> (2019).
33. S. Hu, L. Eberhard, J. Chen, J. C. Love, J. P. Butler, J. J. Fredberg, G. M. Whitesides, and N. Wang, "Mechanical anisotropy of adherent cells probed by a three-dimensional magnetic twisting device," *Am. J. Physiol. - Cell Physiol.* **287**(5), C1184–C1191 (2004).
34. E. Peeters, "Biomechanics of Single Cells Under Compression: Proefschrift," Ph.D. thesis, Technische Universiteit Eindhoven (2004).
35. T. C. Ting and T. Chen, "Poisson's ratio for anisotropic elastic materials can have no bounds," *Q. J. Mech. Appl. Math.* **58**(1), 73–82 (2005).
36. K. W. Wojciechowski, "Poisson's ratio of anisotropic systems," *Comput. Methods Sci. Technol.* **11**(1), 73–79 (2005).

37. W. Rasband, "Voxel Counter: ImageJ Plugins," <https://imagej.nih.gov/ij/plugins/voxel-counter.html> (2002).
38. K. Buschow, R. Cahn, M. Flemings, B. Ilschner, E. Kramer, S. Mahajan, and P. Veysiere, *Encyclopedia of Materials: Science and Technology* (Elsevier Ltd, Amsterdam, 2001).
39. T. D. Visser, F. C. Groen, and G. J. Brakenhoff, "Absorption and scattering correction in fluorescence confocal microscopy," *J. Microsc.* **163**(2), 189–200 (1991).
40. G. N. Greaves, A. L. Greer, R. S. Lakes, and T. Rouxel, "Poisson's ratio and modern materials," *Nat. Mater.* **10**(11), 823–837 (2011).
41. M. C. Jamur and C. Oliver, "Permeabilization of cell membranes," *Methods Mol. Biol.* **588**, 63–66 (2010).
42. A. Boccaccio, M. C. Frassanito, L. Lamberti, R. Brunelli, G. Maulucci, M. Monaci, M. Papi, C. Pappalettere, T. Parasassi, L. Sylla, F. Ursini, and M. De Spirito, "Nanoscale characterization of the biomechanical hardening of bovine zona pellucida," *J. R. Soc. Interface* **9**(76), 2871–2882 (2012).
43. Y. Murayama, C. E. Constantinou, and S. Omata, "Micro-mechanical sensing platform for the characterization of the elastic properties of the ovum via uniaxial measurement," *J. Biomechanics* **37**(1), 67–72 (2004).
44. M. Papi, L. Sylla, T. Parasassi, R. Brunelli, M. Monaci, G. Maulucci, M. Missori, G. Arcovito, F. Ursini, and M. De Spirito, "Evidence of elastic to plastic transition in the zona pellucida of oocytes using atomic force spectroscopy," *Appl. Phys. Lett.* **94**(15), 153902 (2009).
45. D. Manalili, "Raw data from oocyte measurements," figshare (2021) [retrieved 26 October 2021], <https://doi.org/10.6084/m9.figshare.18418415>.